Optically CW-Induced Losses in Semiconductor Coplanar Waveguides

WALTER PLATTE AND BERNHARD SAUERER

Abstract—**This paper presents a quasi-static analysis of photoinduced wave attenuation in a continuously illuminated coplanar waveguide transmission line on semiconductor substrate, using a conformal mapping technique. The relevant effects of charge carrier diffusion and surface recombination on photoconductivity and plasma penetration depth have been incorporated into the theory. This finally allows a quantitative estimate of optically induced losses as a function of the various light source and substrate parameters by means of numerically calculated diagrams. In the particular case of small-plasma-depth excitation, an approximate, analytical expression for the light-controlled attenuation constant is presented. Initial experimental results are in relatively good agreement with the theory.**

I. Introduction

WITHIN THE last decade the pulse-induced optical control of microwave or millimeter-wave components has been established as a very attractive and practical technique of high flexibility allowing scope for constructional details. In particular considerable success has been achieved in the field of optoelectronic microwave switching (OMS), where broad-band capability, subnanosecond speed, simplicity of operation, and near-perfect isolation are of primary importance [1]. In most cases of interest, e.g. for the optoelectronic generation of very short microwave or millimeter-wave bursts [2]–[5] or for optoelectronic sampling [6]–[8], small gap-structure MIC devices on a semiconductor or semi-insulating substrate at low-duty pulsed excitation have been used. As the pulse widths of the applied laser pulses are predominantly much smaller than the excess carrier lifetime of the semiconductor material used, carrier diffusion and surface recombination effects may be neglected; hence the dc and microwave performances of OMS devices have commonly been calculated by means of the well-known lumped-element analysis [1]–[3].

For some time now, increasingly active interest in quasi-CW or even purely CW-induced optical control of MIC components on semiconductor substrate has been observed. This is primarily due to the prospect of novel components or devices, especially with regard to MIC measurements. For example it should be possible in the near future to realize an optically controlled coplanar waveguide sliding termination where the intensity-graded top-side CW excitation generates a smoothly tapered absorbing plasma wedge capable of being moved optoelectronically. Such a device would represent the CW version of the pulse-induced edge-excited optoelectronic microwave load reported previously [9]–[11]. In addition, the recent advance of laser diode and LED array technology with respect to the CW optical output power contributes considerably to the growing interest in this topic.

For estimating the applicability of CW-light-controlled transmission line sections to innovative instrumentation and measurement techniques, the optically induced increase in attenuation of a semiconductor coplanar waveguide line is quantitatively analyzed by means of a conformal mapping technique. In consequence of the CW illumination, the strong influence of carrier diffusion and surface recombination processes on the induced photoconductivity and the plasma penetration depth has to be considered. This implies calculation of the attenuation of a microwave signal propagating through semiconductor material having two-dimensionally inhomogeneous photoconductivity. The results are presented partly in the form of analytical expressions which are applicable within a wide range of relative dielectric constants and characteristic impedances, and partly in the form of specific diagrams referred to a 50 Ω coplanar transmission line on Si, GaAs, and InP substrates.

II. Quasi-Static Analysis of Semiconductor Coplanar Waveguide

A. Conformal Mapping Method

The coplanar waveguide (CPW) configuration to be analyzed is shown in Fig. 1(a), where the semiconductor substrate thickness is assumed to be sufficiently large, and hence can be considered infinite in the analytical model. The ground planes are assumed to be infinitely wide and, in addition, the strip and the ground plane metallization thickness t is considered negligible. Supposing a uniform top-side CW laser irradiance across the slot width W, and neglecting carrier diffusion and surface recombination effects for the present, the excited regions below the air–semiconductor boundary of the slots may be considered approximately as small plasma strips of rectangular cross section $W \times d$, where $W = b_1 - a_1$ is the plasma strip width and d is the plasma penetration depth. The conduc-

Manuscript received January 21, 1988; revised May 31, 1988.

W. Platte is with the Institut fuer Hochfrequenztechnik, Universitaet Erlangen–Nuernberg, D-8520 Erlangen, West Germany.

B. Sauerer is with Messerschmitt–Boelkow–Blohm GmbH, D-8000 Muenchen 80, West Germany.

IEEE Log Number 8823259.

0018-9480/89/0100-0139$01.00

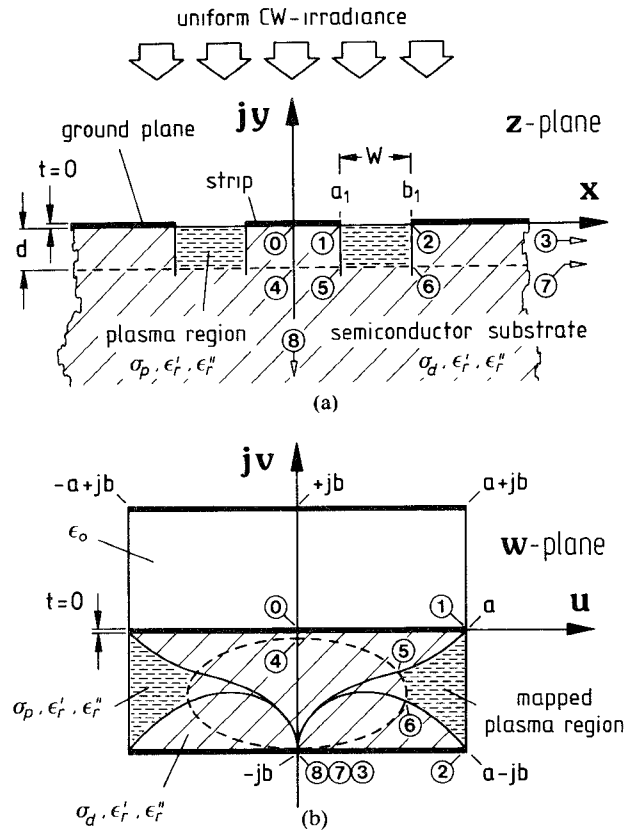

Fig. 1. Conformal transformation planes for CPW analysis. (a) Real configuration of top-side CW-illuminated CPW on semiconductor substrate. (b) Equivalent parallel-plate capacitor model.

tivity σ_p of the plasma strips is assumed to be homogeneous and is $\sigma_p = \sigma_d + \Delta\sigma$, where σ_d is the dark conductivity of the semiconductor substrate and $\Delta\sigma$ is the induced photoconductivity.

The Schwarz–Christoffel transformation mapping the lower half of the z plane into the interior of the lower rectangle in the w plane (Fig. 1(b)), with conductor surface on the top and the bottom and air–semiconductor interfaces on the sides, is given by [12], [13]

$$w = u + jv = \int_0^{z_1} \frac{A\,dz}{\sqrt{z^2 - a_1^2}\sqrt{z^2 - b_1^2}} \tag{1}$$

where A is a constant, a_1 and b_1 denote the specific strip and slot dimensions of the CPW as shown in Fig. 1(a), and $z_1 = x_1 + jy_1$ describes the point to be transformed. Likewise the upper half of the z plane is transformed into the upper rectangle of the w plane. Both rectangles may be considered parallel-plate capacitors of equal electrode width $2a$ and equal plate spacing b, connected in parallel. The ratio a/b can be conveniently expressed as [14]

$$a/b = K(k)/K'(k) \tag{2}$$

where $K(k)$ is the (tabulated) complete elliptic integral of the first kind with modulus $k = a_1/b_1$, and $K'(k) = K(k')$ with $k' = (1 - k^2)^{1/2}$. Accurate and simple analytical expressions for the ratio K/K' as a function of k are available in the literature [15].

Assuming sufficiently small laser irradiance, the influence of the optically induced excess carriers on the electric and magnetic field configurations is of secondary importance.[1] In this case, the total line capacitance per unit length C', including the empty space half-plane, may be written as [14]

$$C' = C_r' + C_0' = 2\epsilon_0(\epsilon_r' + 1)a/b = 2\epsilon_0(\epsilon_r' + 1)K(k)/K'(k) \tag{3}$$

where C_r' refers to the semiconductor-loaded capacitor and C_0' to the air capacitor.

The quasi-static characteristic impedance Z_l for the quasi-TEM mode propagating in the CPW line is then given by [14]

$$Z_l^{\mathrm{CPW}} = \frac{Z_0}{4\sqrt{\epsilon_{re}}} \cdot \frac{K'(k)}{K(k)} \tag{4}$$

where ϵ_{re} is the effective dielectric constant of the CPW according to $\epsilon_{re} = (\epsilon_r' + 1)/2$, ϵ_r' is the real part of the relative permittivity, ϵ_0 is the free-space permittivity, and $Z_0 = 120\pi\ \Omega$ is the intrinsic impedance of free space. Equation (4), in conjunction with the analytical expression for K/K' [15], enables the k value to be calculated for a given set of Z_l and ϵ_r'. For example, considering a 50 Ω CPW line on Si ($\epsilon_r' = 11.7$), GaAs ($\epsilon_r' = 12.9$), or InP ($\epsilon_r' = 12.55$) substrate, one obtains $k_{\mathrm{Si}} = 0.462$, $k_{\mathrm{GaAs}} = 0.424$, and $k_{\mathrm{InP}} = 0.434$.

In order to transform the plasma regions or, more generally, the mesh of orthogonal lines and boundaries within the cross section of the semiconductor substrate (where specific points have been labeled ①, ②, ③, etc., Fig. 1(a)), the elliptic integral (1) has to be solved with complex arguments. For this purpose the z values have been normalized to a_1, i.e., $z' = z/a_1 = x/a_1 + jy/a_1$. Then by substituting $z_1' = x_1' + jy_1' = \sin\varphi_1 = \sin(\phi_1 + j\theta_1)$, the elliptical integral can be rewritten in the form

$$w' = u' + jv' = \frac{w}{a_1} = \frac{A}{a_1 b_1}\int_0^{\varphi_1} \frac{d\varphi}{\sqrt{1 - k^2\sin^2\varphi}} = \frac{A}{a_1 b_1} F(\varphi_1, k) \tag{5}$$

where $F(\varphi_1, k)$ is an incomplete elliptic integral of the first kind with complex amplitude $\varphi_1 = \phi_1 + j\theta_1$ and modulus k, and $A/a_1 b_1$ is a scale factor which has been chosen to be unity in the following analysis to obtain $a/a_1 = K(k)$ and $b/a_1 = K'(k)$, without affecting generality. The transformation proceeds by separating $F(\varphi_1, k)$ into real and imaginary parts according to

$$w' = F(\phi_1 + j\theta_1, k) = F(\alpha_1, k) + jF(\beta_1, k'). \tag{6}$$

The numerical evaluation of the modified amplitudes α_1

[1] For a more rigorous approach, dielectric relaxation and space charge effects have to be considered, particularly in the case of semi-insulating material. However this would imply a considerable increase in complexity of both the carrier transport and the wave propagation analysis, and hence has been disregarded for this quasi-static approximation.

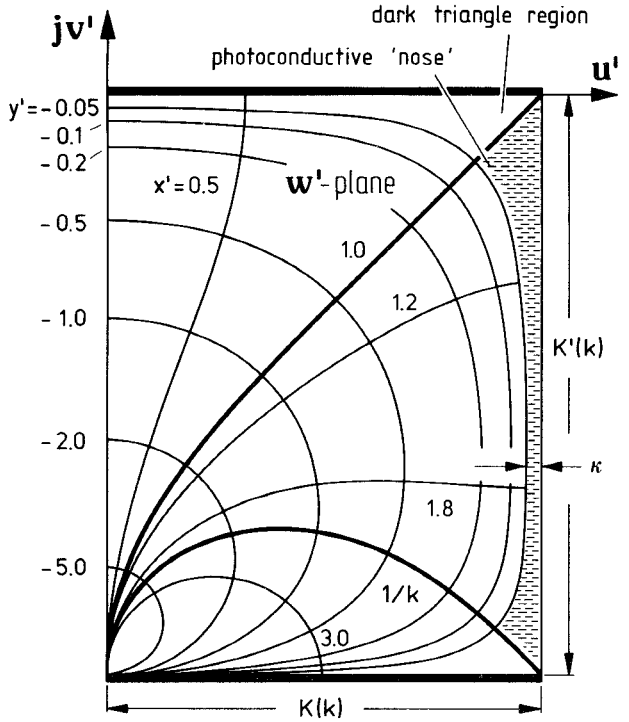

Fig. 2. Actual distribution of $x' =$ constant and $y' =$ constant lines within the right-hand half of the lower rectangle in the w' plane, calculated for a 50 Ω CPW configuration on silicon substrate ($k = 0.462$).

and β_1 can be accomplished in reasonably straightforward fashion by means of the following equations [16]:

$$\cot^4\alpha_1 - \left[\cot^2\phi_1 + k^2\sinh^2\theta_1\csc^2\phi_1 - (1-k^2)\right]\cot^2\alpha_1 - (1-k^2)\cot^2\phi_1 = 0 \tag{7}$$

$$k^2\tan^2\beta_1 = \tan^2\phi_1\cot^2\alpha_1 - 1 \tag{8}$$

where ϕ_1 and θ_1 can easily be calculated from the relations $x_1' = \cosh\theta_1\sin\phi_1$ and $y_1' = \sinh\theta_1\cos\phi_1$, referring to the above substitution. Since the CPW configuration is symmetric with respect to the vertical plane at $x = 0$, only one half ($x \geqq 0$) of the structure needs to be considered for the purpose of conformal mapping.

As a result the specific shape of the transformed plasma region and its position within the lower rectangle in the w plane are qualitatively shown in Fig. 1(b). An accurate plot of a mapped 50 Ω CPW configuration on silicon substrate ($k = 0.462$) is presented in Fig. 2, exhibiting the actual distribution of $x' =$ constant and $y' =$ constant lines in the w' plane.

B. General Calculation of Wave Attenuation

Wave attenuation in a photoexcited CPW line on semiconductor substrate is caused by four loss components: conductor losses (α_c), dielectric losses (α_ϵ), dark-conductivity losses (α_d), and photoconductivity losses (α_{ph}). Hence, the total attenuation constant α^{CPW} may be written as

$$\alpha^{CPW} = \alpha_c + \alpha_\epsilon + \alpha_d + \alpha_{ph}. \tag{9}$$

When a quasi-static approximation is valid, one can use Wheeler's incremental inductance rule for evaluating conductor (ohmic) losses. An analytical expression for α_c is available in the literature [14].

Dielectric losses in CPW lines are usually calculated from [14]

$$\alpha_\epsilon = \frac{\omega\epsilon_0\epsilon_r' Z_0}{4\sqrt{\epsilon_{re}}}\tan\delta_\epsilon = 13.64\frac{f\epsilon_r'}{c_0\sqrt{\epsilon_{re}}}\tan\delta_\epsilon \quad \text{dB/unit length} \tag{10}$$

where c_0 is the velocity of light in free space, f is the signal frequency with $\omega = 2\pi f$, and $\tan\delta_\epsilon = \epsilon_r''/\epsilon_r'$ is the "polarization loss tangent" of the semiconductor substrate. It should be noted that (10) is based on the assumption of small losses, i.e., $\tan\delta_\epsilon \ll 1$. In addition a filling fraction of 0.5 for the CPW has been assumed.

Similarly, the losses due to substrate conductivity can be determined from (10) by replacing $\tan\delta_\epsilon$ by the conductivity loss tangent $\tan\delta_\sigma = G'/\omega C_r'$, where G' is the total conductance per unit length of the parallel-plate capacitor model (Fig. 1(b)) and $C_r' = 2\varepsilon_0\epsilon_r' a/b$ according to (3). This substitution finally results in

$$\alpha_d + \alpha_{ph} = \frac{Z_0 G'}{8\sqrt{\epsilon_{re}}}\cdot\frac{b}{a} = \frac{Z_0 G'}{8\sqrt{\epsilon_{re}}}\cdot\frac{K'(k)}{K(k)} \tag{11}$$

again assuming small losses, i.e., $G' \ll \omega C_r'$. If no excitation occurs the conductivity losses are governed merely by the dark conductivity σ_d of the substrate. Thus, one obtains $\alpha_{ph} = 0$ and $G' = 2\sigma_d a/b$, yielding

$$\alpha_d = Z_0\sigma_d/4\sqrt{\epsilon_{re}} = 2.17 Z_0\sigma_d/\sqrt{\epsilon_{re}} \quad \text{dB/unit length.} \tag{12}$$

In the case of excitation, an inhomogeneous distribution of conductivity is built up within the lower rectangle in the w' plane according to $\sigma(u', v') = \sigma_d + \Delta\sigma(u', v')$, where for the present the induced photoconductivity $\Delta\sigma(u', v')$ is piecewise uniform because of the assumptions mentioned in subsection II-A.

In order to obtain the optically induced (net) increase in attenuation explicitly as a function of light source and substrate parameters, it is very useful to separate photoconductivity losses and dark-conductivity losses. This can be achieved by utilizing a capacitor substitution as shown in Fig. 3, where the right-hand half of the mapped CPW configuration is finally replaced by a capacitor of normalized electrode width $a/a_1 = K(k)$ with uniform dark conductivity σ_d and a fictitious shunt capacitor of normalized electrode width s with uniform photoconductivity $\Delta\sigma$. Thus, G' may be written in the form $G' = G_d' + \Delta G'$ with $G_d' = 2\sigma_d K(k)/K'(k)$ and $\Delta G' = 2\Delta\sigma s/K'(k)$, which finally enables the photoconductivity losses to be expressed separately as an additive term α_{ph} in (9) according to

$$\alpha_{ph} = \frac{Z_0\Delta\sigma}{4\sqrt{\epsilon_{re}}}\cdot\frac{s}{K(k)} = 2.17\frac{Z_0\Delta\sigma}{\sqrt{\epsilon_{re}}}\cdot\frac{s}{K(k)} \quad \text{dB/unit length.} \tag{13}$$

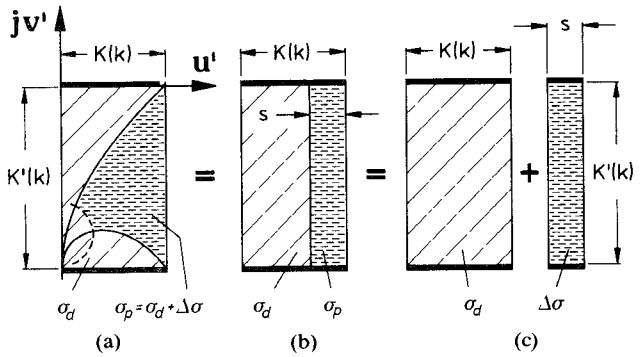

Fig. 3. Replacement of (a) mapped CPW configuration by (b) an equivalent two-section capacitor with uniform conductivities σ_d and σ_p, respectively, and (c) its final separation for the analysis.

As the curved interface lines between the dark and the excited regions cannot be described in a closed analytical form, and hence G' cannot be expressed in terms of simple functions, in general the evaluation of α_{ph} has to be accomplished numerically.

C. Optically Induced Attenuation at Small Plasma Depths

When considering very thin plasma strips of normalized plasma depth $\delta \ll 1$, where $\delta = d/a_1$ (Fig. 1(a)), and supposing $0.2 \leqq k \leqq 0.8$ (which covers the wide scope of CPW configurations for actual and future applications with respect to Z_l and ϵ_r'), the mapped plasma region appears as a narrow and elongated quasi-rectangular shunt zone of normalized minimum width $\kappa \ll K'(k)$ with two triangle-like "noses." This can be verified from Fig. 2, where the shadowed area, for example, represents the photoconductive shunt zone in the case of $y' = -\delta = -0.05$.

Motivated by the presumption that it should be possible to find an analytical approximation of s as a function of δ, k and contrast ratio $\nu = \Delta\sigma/\sigma_d$, at least at the aforementioned condition of small plasma depths, the influences of the photoconductive noses and of the dark triangle regions (between electrode and photoconductive shunt zone) on the total parallel-plate conductance G' have been studied analytically by means of the simplified configuration shown in Fig. 4(c) [17], [18]. The essential results of this analysis can be summarized as follows. Owing to the effect of lateral carrier diffusion (see Section III), the "dark" triangle regions are actually flooded by excess carriers from the plasma region, and hence become photoconductive too. Bearing in mind that an effective increase in conductivity because of diffusion is only obtained across a distance equal to the ambipolar diffusion length L_a (Fig. 4(a)), the dark triangle regions are sufficiently photoconductive, and consequently may be entirely incorporated into the plasma shunt zone $\kappa \times K'(k)$ if $\kappa \leqq \eta_{1,2}$, where η_1 and η_2 are the normalized widths of the mapped diffusion zones (Fig. 4(b)). As $\eta_1 > \eta_2$, due to the conformal mapping, $\kappa \leqq \eta_2$ is the stronger requirement, so the condition for nonaffecting triangle regions can be written as

$$\kappa \leqslant K(k) - F\left(\arcsin\frac{1}{1+kL_a/a_1}, k\right). \tag{14}$$

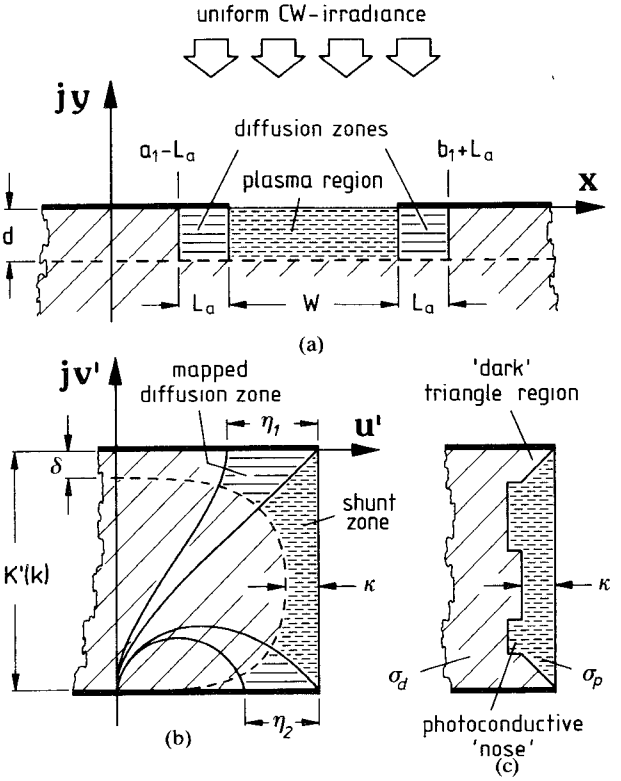

Fig. 4. (a) Actual position and shape of the plasma region and its diffusion zones, (b) equivalent parallel-plate configuration at small-plasma-depth condition, and (c) a simplified model for the analysis.

Moreover, s has been found to depend on the total area $A_n(\delta, k)$ of the two photoconductive noses, weighted by the contrast ratio ν. As a result, the simplified-model analysis yields

$$s(\delta, k, \nu) \simeq \kappa\left[1 + \frac{A_n(\delta, k)}{1+\nu B}\right] \tag{15a}$$

with

$$A_n(\delta, k) \simeq A(\delta) k^{m(\delta)} \tag{15b}$$

and

$$\kappa \simeq D(k)\delta \tag{15c}$$

where $A(\delta)$ is a fifth-degree polynomial, $m(\delta)$ and $D(k)$ are correction factors, and B is a constant.

Referring to (15a) and (15c), the simple relation $s \simeq \kappa \simeq D(k)\cdot\delta$ is obtained at the high-excitation condition ($\nu \gg 1$), which agrees exactly with the physical situation in the parallel-plate configuration.

In addition, the exact structure (Fig. 4(b)) has been investigated by means of a computer analysis. The corresponding numerical results then have been utilized to specify $A(\delta)$, $m(\delta)$, $D(k)$, and B for the purpose of best fit as follows [17]:

$$A(\delta) \simeq A_5(\log\delta)^5 + \cdots + A_1(\log\delta) + A_0 \tag{15d}$$

with

$A_5 = -0.035279$, $A_4 = -0.516164$, $A_3 = -3.046445$,

$A_2 = -8.532793$, $A_1 = -11.475891$, and $A_0 = -5.478049$,

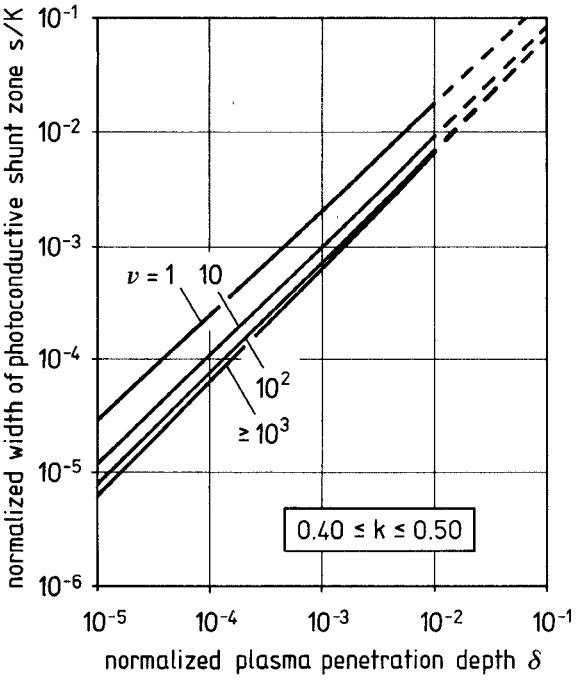

Fig. 5. Plot of normalized width s/K of photoconductive shunt zone as a function of normalized plasma penetration depth δ with contrast ratio ν as parameter (small-plasma-depth approximation). The curves apply to 50 Ω CPW transmission lines on GaAs, InP, and Si substrates ($0.40 \leqq k \leqq 0.50$).

and

$$m(\delta) \simeq 0.08 \log \delta - 0.77 \tag{15e}$$

$$D(k) \simeq \tan(1.56k + 0.115) \tag{15f}$$

$$B \simeq 0.89 \tag{15g}$$

In conclusion, when evaluating the photoinduced attenuation α_{ph} from (13) and (15) in consideration of (14), an overall accuracy of at least 28 percent is obtained, supposing $10^{-5} \leqq \delta \leqq 10^{-2}$, $0.2 \leqq k \leqq 0.8$, and $1 \leqq \nu \leqq \infty$. As an example Fig. 5 shows the ratio s/K as a function of δ with ν as parameter, originally calculated for a 50 Ω CPW transmission line on a silicon substrate ($k = 0.462$). Moreover these curves apply practically within the range $0.40 \leqq k \leqq 0.50$ (thus including 50 Ω CPW lines on GaAs and InP substrates), because a corresponding change in k leads to only a small change of s/K which is less than or equal to the line width. The broken curves indicate an extrapolation which indeed is quite obvious, but is not included in the small-plasma-depth analysis.

III. Analysis of Optoelectronic Performance

A. Diffusion-Controlled Distribution of Photoconductivity

In the case of optical CW excitation, the distribution of photoconductivity within the plasma region and its near environment is strongly influenced by carrier diffusion and surface recombination processes, and hence is really inhomogeneous. For a rigorous analysis of these mechanisms, the two-dimensional continuity equation for the induced excess carrier concentration would have to be solved in conjunction with some boundary conditions which are

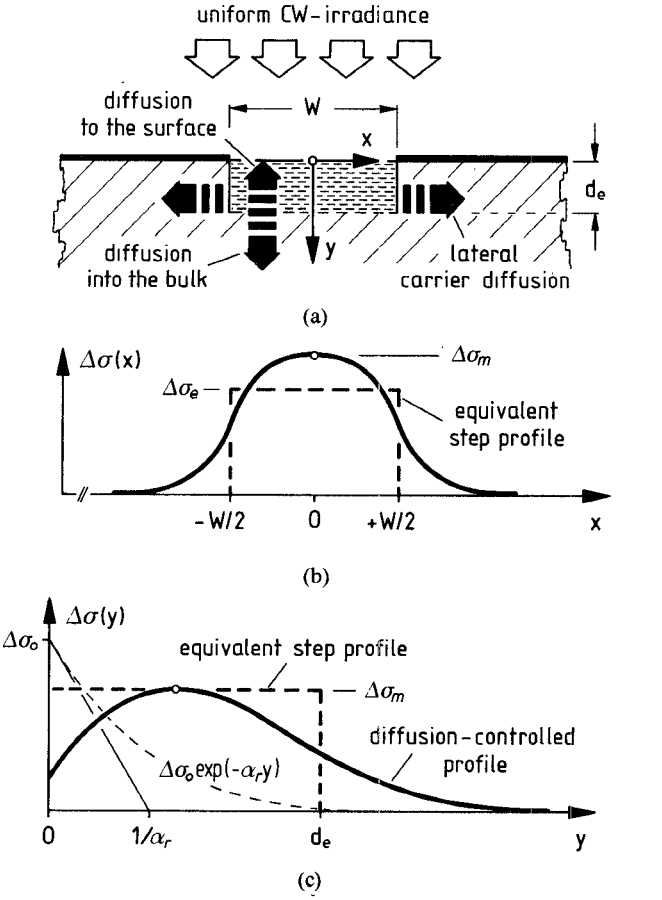

Fig. 6. (a) Cross-sectional view of optically excited CPW slot region, (b) the corresponding lateral distribution of photoconductivity $\Delta\sigma(x)$, and (c) the profile $\Delta\sigma(y)$ generated perpendicularly to the illuminated surface.

usually difficult to measure. This, however, would finally result in relatively complex equations of little practical advantage.

Therefore this section refers to a simplified, experimentally confirmed analysis [19] where the two-dimensional distribution of photoconductivity $\Delta\sigma(x, y)$ has been approximated by the product of the separate profiles $\Delta\sigma(x)$ and $\Delta\sigma(y)/\Delta\sigma_0$, each calculated from an idealized excitation model with perfect one-dimensional carrier flow.

When considering the cross-sectional slot region of a CPW line of the type shown in Fig. 6(a), where the coordinate system has been placed in the middle of the gap, and furthermore supposing a trapless single-crystal material, a uniform CW irradiance across the gap, a quasi-neutral excess carrier generation, no carrier flow in the y direction, and negligible contact recombination at the strip and the ground plane metallization, the diffusion-controlled profile $\Delta\sigma(x)$ is approximately given by [19], [20]

$$\Delta\sigma(x) = \Delta\sigma_m \left[1 - \exp(-W/2L_a)\cosh(x/L_a)\right], \quad 0 \leqq x \leqq W/2 \tag{16a}$$

$$\Delta\sigma(x) = \Delta\sigma_m \sinh(W/2L_a)\exp(-x/L_a), \quad W/2 \leqq x \leqq \infty \tag{16b}$$

with

$$L_a = \left[(2\mu_n\mu_p\tau k_B T/q)(\mu_n+\mu_p)^{-1}\right]^{1/2}. \quad (16c)$$

W is the gap width, L_a is the ambipolar diffusion length, $\Delta\sigma_m$ is the maximum photoconductivity at $x=0$, μ_n and μ_p are the mobilities of electrons and holes, τ is the excess carrier lifetime, k_B is Boltzmann's constant, T is the absolute temperature, and q is the electronic charge. Carrier lifetime and mobilities are assumed to be independent of excess carrier density. A typical shape of $\Delta\sigma(x)$ is shown in Fig. 6(b). It is seen that the lateral carrier diffusion causes a significant loss of photoconductivity at the ends of the illuminated gap zone, which can drastically reduce the effective gap (or parallel-plate) conductance G' (subsections II-B and II-C).

Concerning the profile $\Delta\sigma(y)$, a negligible carrier flow in the x direction is now supposed. All other assumptions mentioned above apply, and $\Delta\sigma(y)$ then may be expressed as [21], [22]

$$\Delta\sigma(y) = \frac{\Delta\sigma_0}{(1-\alpha_r^2 L_a^2)} \cdot\left[\exp(-\alpha_r y) - \frac{\alpha_r L_a^2 + v_s\tau}{L_a + v_s\tau}\exp(-y/L_a)\right], \quad 0 \leqq y \leqq \infty \quad (17a)$$

with

$$\Delta\sigma_0 = (q/hc_0)(\mu_n+\mu_p)(1-R)\alpha_r S\lambda_p \tau P/A \quad (17b)$$

where $\alpha_r(\lambda)$ is the radiation absorption coefficient, which strongly depends on optical wavelength λ [3], v_s is the surface recombination velocity, h is Planck's constant, and c_0 is the velocity of light in free space. $R(\lambda)$ is the surface reflectivity, and $S(\lambda)$ is the relative spectral response of the semiconductor material exhibiting a peak response at the optical wavelength λ_p [3]. P is the incident optical power and A is the illuminated area. Moreover the internal quantum efficiency of the semiconductor material has been assumed to be unity, which corresponds to perfectly intrinsic photogeneration (of electron–hole pairs exclusively).

It is seen from (17a) that $\Delta\sigma(y)$ results from the superposition of an absorption term which is proportional to $\exp(-\alpha_r y)$, and a v_s-controlled diffusion term which is proportional to $\exp(-y/L_a)$. The general shape (Fig. 6(c)) is characterized by the typical loss of photoconductivity within the surface region and, on the other hand, by a relatively large plasma depth, which can exceed the optical penetration depth $1/\alpha_r$. This illustrates well the influence of surface recombination and carrier diffusion.

B. Effective Photoconductivity and Plasma Depth

To take advantage of the results presented in Section I, where the actually inhomogeneous distribution of photoconductivity has been replaced by a piecewise-uniform one as a first-order approximation, the quasi-real profile $\Delta\sigma(y)$ can be replaced by a step profile of constant photoconductivity $\Delta\sigma_m$ which extends over an effective plasma penetration depth d_e (Fig. 6(c)), according to [19]

$$\Delta\sigma_m = \frac{\Delta\sigma_0}{(1+\alpha_r L_a)}\left[\frac{1}{\alpha_r L_a}\left(\frac{\alpha_r L_a^2 + v_s\tau}{L_a + v_s\tau}\right)\right]^{-\alpha_r L_a/(1-\alpha_r L_a)} \quad (18)$$

and

$$d_e = \frac{1}{\alpha_r}\left[\frac{L_a(1+\alpha_r L_a)+v_s\tau}{L_a+v_s\tau}\right] \cdot\left[\frac{1}{\alpha_r L_a}\left(\frac{\alpha_r L_a^2+v_s\tau}{L_a+v_s\tau}\right)\right]^{\alpha_r L_a/(1-\alpha_r L_a)}. \quad (19)$$

A discussion of d_e as a function of optical wavelength in terms of $\alpha_r(\lambda)$ shows that $d_e \simeq 1/\alpha_r$ in the long-wavelength region ($\alpha_r L_a \ll 1$) and $d_e \simeq L_a$ in the short-wavelength region ($\alpha_r L_a \gg 1$).

For incorporating also the effect of lateral carrier diffusion into the concept of piecewise-constant photoconductivity, the actual profile $\Delta\sigma(x)$ within the range $-W/2 \leqq x \leqq +W/2$ can be replaced by an effective (uniform) photoconductivity $\Delta\sigma_e$ (Fig. 6(b)), which can be calculated approximately from [19]

$$\Delta\sigma_e \simeq \Delta\sigma_m(W/4L_a)(1-\zeta^2)^{1/2} \cdot\left\{Arth\left[(1-\zeta)/(1+\zeta)\right]^{1/2}\right\}^{-1} \quad (20a)$$

with

$$\zeta = \exp(-W/2L_a). \quad (20b)$$

This expression holds true practically within the wide range of $1 \leqq \nu_m \leqq \infty$ at arbitrary W/L_a, where $\nu_m = \Delta\sigma_m/\sigma_d$, accepting a maximum relative error of 1.6 percent with respect to the exact ν_m-controlled equation [18], [19]. A discussion of $\Delta\sigma_e$ as a function of W/L_a shows that $\Delta\sigma_e/\Delta\sigma_m \simeq 0.5\ W/L_a$ if $W \ll L_a$ (strongly interfering lateral diffusion), and $\Delta\sigma_e/\Delta\sigma_m \simeq 1$ if $W \gg L_a$ (negligible lateral diffusion). In this way, the excited slot regions of a semiconductor CPW line may be regarded as rectangular parallelepiped plasma strips of cross section $W \times d_e$ and homogeneous photoconductivity $\Delta\sigma_e$. Thus the analysis presented in Section II can be used again by substituting $d \to d_e$, $\nu \to \nu_m$, and $\Delta\sigma \to \Delta\sigma_e$. Of course this implies an additional error of up to 30 percent in the worst case of $W \ll L_a$ [17], [18]. Concerning an estimate of α_{ph} as a function of W, it should be noted that δ also depends on W according to $\delta = d_e/a_1$ along with $a_1 = Wk/(1-k)$, and hence the condition $\delta \ll 1$ (Section II) can be violated with decreasing W.

IV. Rigorous Numerical Evaluation of s/K

Discarding both the restriction of very small plasma depths and the assumption of a piecewise-constant photoconductivity, the general computation of α_{ph} and s/K has been accomplished as follows. Initially a mesh of orthogonal lines aligned with the coordinate axes is "drawn" over

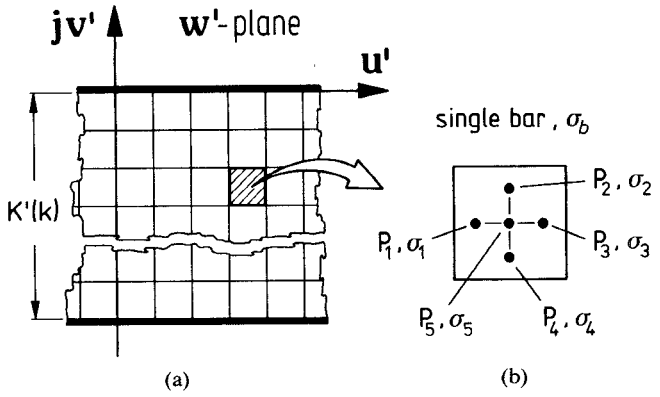

Fig. 7. Parallel-plate capacitor model presented as (a) a row-and-column arrangement of rectangular parallelepiped bars of semiconductor material, and (b) choice positions of the discrete "conductivity points" within the cross section of a single bar.

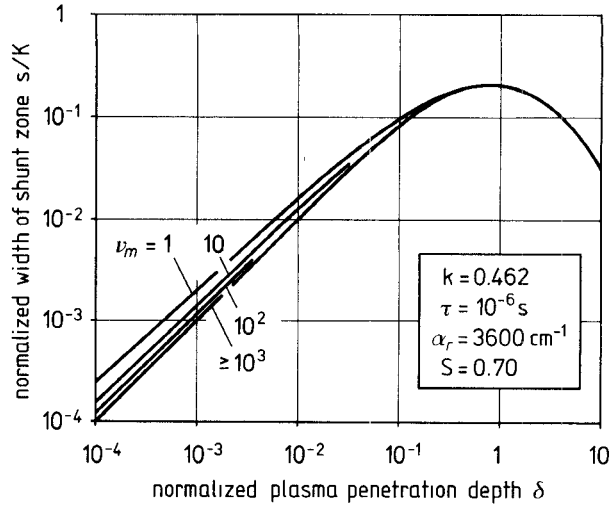

Fig. 8. Plot of normalized width s/K of photoconductive shunt zone as a function of normalized plasma penetration depth δ with maximum contrast ratio ν_m as parameter. Accepting an error of $\leqq 4$ percent, these curves practically apply within the range $0.40 \leqq k \leqq 0.50$ for arbitrary τ and $\alpha_r \geqq 10^3$ cm^{-1}.

the cross-sectional region of the parallel-plate capacitor in the w' plane (Fig. 7). Thus the capacitor may be visualized as a row-and-column arrangement of rectangular parallelepiped bars of semiconductor material connected in parallel. To ensure a sufficiently small mesh width, particularly within the regions of strongly inhomogeneous excitation, the mesh width is reduced with increasing gradient of photoconductivity [17].

Next at five specific points which are cruciformly positioned within the cross section of each bar (and where the distance between the outer points and the mesh line is 20 percent of the mesh width), the actual "point" conductivity σ_n (with $n = 1,2,\cdots,5$ and $\sigma_n = \Delta\sigma_n + \sigma_d$) is determined by inverse conformal mapping of the w' position $P_n(u', v')$ into the corresponding z position $P_n(x, y)$, utilizing the Jacobian elliptic function $\mathrm{am}(F, k)$ [16], [23], and further by calculation of $\Delta\sigma_n$ from $\Delta\sigma(x, y) = \Delta\sigma(\tilde{x}) \cdot \Delta\sigma(\tilde{y})/\Delta\sigma_0$ (Section III). In consequence of the different choices of the coordinate systems shown in Fig. 1(a) and Fig. 6(a), the substitutions $\tilde{x} = x - (a_1 + W/2)$ and $\tilde{y} = -y$ have to be considered also.

Finally, the average (uniform) conductivity σ_b of a single bar is given as the arithmetic mean of the discrete values σ_n, i.e., $\sigma_b = \sigma_d + \sum_{n=1}^{5} \Delta\sigma_n/5$. The total conductance per unit length G' of the parallel-plate capacitor is then calculated by summing all the resistivity contributions of the bars within a single column and, subsequently, summing all the conductivity contributions of the columns. Referring to the capacitor substitution (Fig. 3) used for the separation of α_d and α_{ph} (subsection II-B), $s/K(k)$ can be obtained from

$$\frac{s}{K(k)} = \frac{G'}{2\Delta\sigma_m} \cdot \frac{K'(k)}{K(k)} - \frac{\sigma_d}{\Delta\sigma_m} \tag{21}$$

where the factor $1/2$ in the denominator indicates that only one half ($0 \leqq u' \leqq K$) of the capacitor configuration has been considered for the purpose of numerical evaluation.

Fig. 8 shows the resulting ratio s/K as a function of δ with ν_m as parameter, calculated for a 50 Ω CPW transmission line on silicon substrate ($k = 0.462$, $\tau = 10^{-6}$ s) for He–Ne laser excitation ($\alpha_r = 3600$ cm^{-1}, $S = 0.70$). When comparing these curves with the results obtained from the small-plasma-depth analysis (Fig. 5), it can be seen that in each case the corresponding curves lie very close to each other for $\delta \ll 1$, disregarding an inherent discrepancy factor not exceeding $\sqrt{2}$, which seems to be remarkably small with regard to the approximations used in subsection II-C.

Fig. 9 illustrates the slight second-order dependence of s/K on the absorption coefficient α_r and carrier lifetime τ, for example at $\nu_m \geqq 10^3$. For a correct interpretation of these diagrams it should be recalled that δ itself is a function of α_r and τ according to (19) with $\delta = d_e/a_1$ (first-order dependence). At small plasma depths, i.e., $\delta \leqq 0.1$, the ratio s/K obviously exhibits no second-order dependence on α_r or τ, whereas for $\delta > 0.1$ there is an evident second-order dependence on α_r, which is additionally sensitive to τ at small absorption coefficients $\alpha_r \leqq 10^3$ cm^{-1}. Moreover, concerning the overall performance of the photoinduced attenuation constant α_{ph} as a function of α_r and τ, it should be noted that α_{ph} explicitly depends on $\Delta\sigma$ (or $\Delta\sigma_e$), which is also sensitive to α_r and τ according to (20), (18), (17b) and (16c).

Likewise, the ratio s/K of a 50 Ω CPW line on GaAs as well as on InP substrate has been computed, resulting in similar diagrams which in the most interesting case of $\alpha_r \geqq 10^3$ cm^{-1} practically agree (error: $\leqq 4$ percent) with those shown in Fig. 9. Hence, the set of curves presented in Fig. 8 can be used successfully within the range $0.40 \leqq k \leqq 0.50$ (see subsection II-C) for arbitrary τ and $\alpha_r \geqq 10^3$ cm^{-1}. Of course this behavior considerably simplifies the evaluation of optically induced losses. It is primarily due to (i) the special presentation of s/K as a function of $\delta(\tau, \alpha_r, v_s, k, W)$, (ii) the choice of α_r as parameter instead

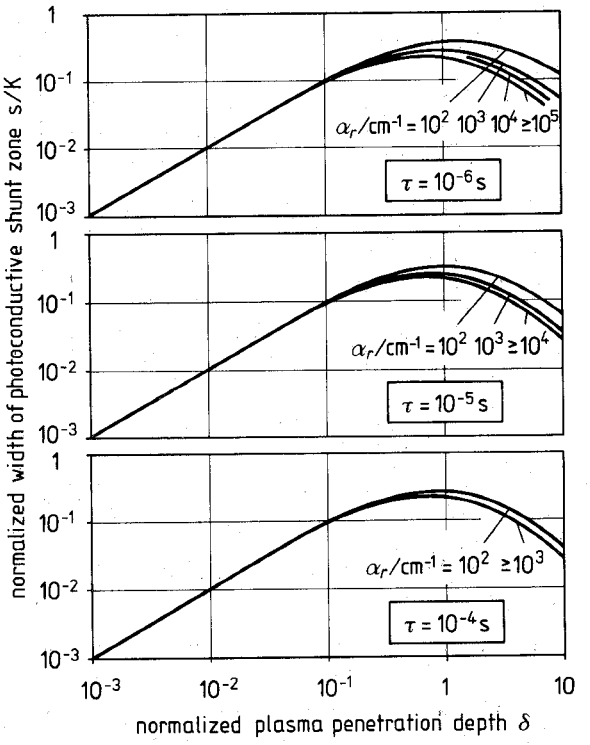

Fig. 9. Illustrative presentation of the slight second-order dependence of normalized width s/K on radiation absorption coefficient α_r and carrier lifetime τ in the case of $k = 0.462$ and $\nu_m \geqq 10^3$.

of the optical wavelength λ, and (iii) the fact that the influence of $R(\lambda)$ and $S(\lambda)$ on s/K is only of secondary importance with respect to the influence of $\alpha_r(\lambda)$.

Finally it is interesting to note that the maximum value of s/K appears for $\delta \simeq 1$, where the effective plasma penetration depth is equal to or close to half the strip width.

V. Experimental Results

The experimental results reported here have been obtained from a 50 Ω CPW transmission line on silicon substrate measuring 2.54 cm × 2.54 cm × 0.05 cm and mounted in a CPW test fixture as shown in Fig. 10. The substrate parameters were $\epsilon_r' = 11.7$, $\sigma_d = 2.5 \times 10^{-4}$ $(\Omega \cdot \text{cm})^{-1}$, $\tau = 10^{-6}$ s, $L_a = 47$ μm, $(\mu_n + \mu_p) = 2100$ cm^2/Vs, $v_s = 10^2$ cm/s, $R = 0.30$, and $\lambda_p = 860$ nm (manufacturer's specification sheet: Siemens AG, Munich). The Au metallization thickness was about 7 μm.

The device under test was a trisection CPW structure which consisted of a normal line section (i.e., the actual test section, strip width $2a_1 = 1200$ μm, slot width $W = 700$ μm, line length $l = 10$ mm) and two taper sections (with $2a_1 = 515$ μm and $W = 300$ μm at the substrate edge) for proper adaptation of the CPW dimensions to the SMA connector dimensions, so maintaining $Z_l = 50$ Ω. To realize a greater effective substrate thickness (which has been assumed infinite for the analysis), the aforementioned test specimen was actually mounted on a "pile" of three further silicon substrates of 0.05 cm thickness each [25].

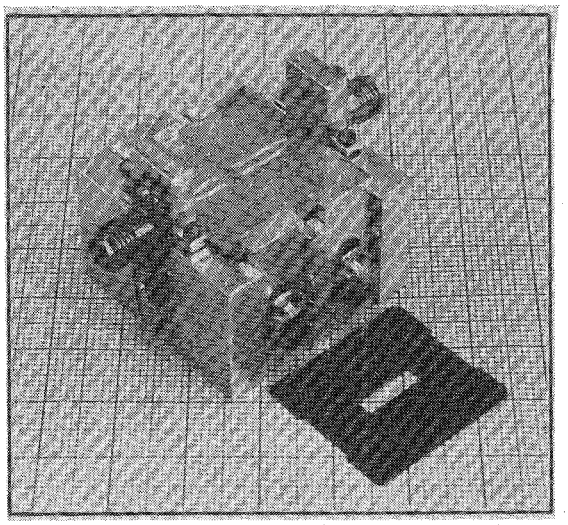

Fig. 10. Photograph of silicon CPW transmission line mounted in a CPW test fixture, and black paper mask.

Moreover, the test section was mask-limited to prevent any excitation of the taper sections.

In a first experiment (A), the CPW line was illuminated by a 40 mW He–Ne laser ($\lambda = 633$ nm) which was adjusted at a suitable spread of beam for realizing a nearly homogeneous (effective) irradiance of about 30 mW/cm^2 across the test aperture measuring 10 mm × 2.6 mm.

In a second experiment (B), the test section was illuminated by six 50 mW LED's (Hitachi HLP 50 RC, $\lambda = 834 \cdots 854$ nm), each coupled to a noncoherent glass fiber bundle of about 40 cm length using 460 individual step-index fibers in parallel. At their output ends, the six bundles were potted in an epoxy resin molding in such a way that two rectangular output faces of 0.7 mm × 10 mm, arranged like a sign of equality, with 1.2 mm spacing between them could be realized. Thus, the fiber bundle configuration was used as a shape-changing light guide system ("circle-to-slit" transformation) to match the six LED beam cross sections to the CPW areas to be illuminated [25]. Owing to separate driver circuits, the currents through the LED's could individually be adjusted in order to produce a quasi-homogeneous irradiance of 30 mW/cm^2 as well.

In a third experiment (C), the LED's were then operated at their rated current value of 200 mA, thereby producing an irradiance of 357 mW/cm^2 at the semiconductor surface. In this case, the molding head was positioned with its shortest possible distance to the substrate, given by the 140 μm thickness of the black paper mask [25].

The measurement of photoinduced attenuation was easily performed by means of a simple power meter (hp 432A), which made it possible to read small changes in attenuation with a resolution of 0.05 dB after adjusting the meter to the 0 dB dark-state full-scale value for each measuring point.

As a result, Fig. 11 shows the photoinduced insertion loss L_{ph} of the silicon CPW test section versus signal frequency f under the excitation conditions A, B, and C

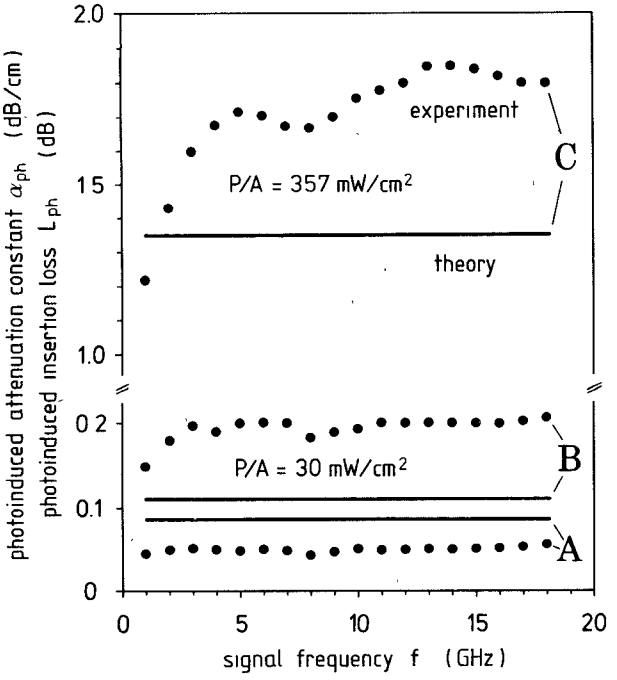

Fig. 11. Photoinduced insertion loss L_{ph} and photoinduced attenuation constant α_{ph} of silicon CPW test section versus signal frequency f in the case of He–Ne laser excitation (A) and IR-LED excitation (B,C). (A): He–Ne laser excitation, $\lambda = 633$ nm, $P/A = 30$ mW/cm^2. (B): IR-LED excitation, $\lambda = 840$ nm, $P/A = 30$ mW/cm^2. (C): IR-LED excitation, $\lambda = 840$ nm, $P/A = 357$ mW/cm^2. The length of excited CPW section was $l = 1$ cm.

mentioned above. As the experiments were accomplished at sufficiently well realized "matched conditions" (where the impedances of signal source and load are equal to the characteristic impedance Z_l of the dark CPW line), the ordinate scale also allows a direct reading for the photoinduced attenuation constant α_{ph} in dB/cm according to $L_{ph} = \alpha_{ph} \cdot l$ with $l = 1$ cm, supposing uniform excitation across $W \times l$.

Although of slight interest here, the insertion loss of the dark CPW (including the SMA connectors) was measured ranging from 0.8 dB at 1 GHz up to 2 dB at 18 GHz [25]. Moreover, the photoinduced attenuation α_{ph} was measured as a function of forward current I through the LED's, which were series-connected in this case. From the α_{ph}–I characteristic (modulation characteristic), a slight sublinear behavior with increasing current could be observed [25]. This effect can be explained by the theory presented here, bearing in mind that α_{ph} is proportional to $\Delta\sigma$ and s/K, where $\Delta\sigma$ is proportional to P and I, respectively, whereas s/K decreases with increasing ν_m and I, respectively (Fig. 8).

For comparison, the theoretical results are summarized as follows. In the case of He–Ne laser excitation (A), one obtains $\Delta\sigma_m = 4.14 \times 10^{-3}$ $(\Omega \cdot \text{cm})^{-1}$ along with $\alpha_r(\lambda = 633$ nm$) = 3600$ cm^{-1} [24], $S(\lambda = 633$ nm$) = 0.70$ [3] and $P/A = 30$ mW/cm^2, $\nu_m = 16.6$, $d_e = 49.8$ μm, $\delta = 0.0829$, $\Delta\sigma_e = 3.78 \times 10^{-3}$ $(\Omega \cdot \text{cm})^{-1}$, and $s/K = 0.070$ from Fig. 8, which finally yields $\alpha_{ph,A} = 0.086$ dB/cm from (13), using $\epsilon_{re} = 6.35$ and $Z_0 = 377$ Ω.

In the case of low LED excitation (B), one obtains $\Delta\sigma_m = 4.8 \times 10^{-3}$ $(\Omega \cdot \text{cm})^{-1}$ along with $\alpha_r(\lambda = 840$ nm$) = 700$ cm^{-1}, $S(\lambda = 840$ nm$) = 1$ and $P/A = 30$ mW/cm^2, $\nu_m = 19.2$, $d_e = 61.6$ μm, $\delta = 0.1024$, $\Delta\sigma_e = 4.38 \times 10^{-3}$ $(\Omega \cdot \text{cm})^{-1}$, and $s/K = 0.080$, resulting in $\alpha_{ph,B} = 0.11$ dB/cm. High LED excitation (C) with $P/A = 357$ mW/cm^2 finally yields $\Delta\sigma_e = 0.052$ $(\Omega \cdot \text{cm})^{-1}$, $\nu_m = 228$ and $\alpha_{ph,C} = 1.35$ dB/cm. As α_{ph} is approximately insensitive to signal frequency (apart from a slight frequency dependence of ϵ_{re} [14]), the calculated α_{ph} values have been presented as horizontal lines in Fig. 11, for simplicity.

It is seen that, on the whole, the theoretical and experimental results agree fairly well.[2] At frequencies below X-band, however, the curve C of the measured α_{ph} values at high LED excitation exhibits a distinct roll-off with decrease in frequency. This effect can be explained by the fact that, for such a high photoexcitation and sufficiently low frequencies, the CPW is operated under a high-loss condition according to $G' \gtrsim \omega C_r'$, where α_{ph} becomes sensitive to frequency and (10) is no longer valid (see Section VI).

VI. Concluding Remarks

The results presented in this paper are based on the quasi-static analysis with the assumption that the semiconductor substrate acts like a low-loss dielectric and is thick enough to be considered infinite. From this, the fundamental mode of propagation may be regarded as a dielectric quasi-TEM mode. This conventional TEM approximation is valid within a relatively wide frequency range (here up to 20 GHz) where the upper limit is governed by the actual values of ϵ_r', a_1, and b_1 and, of course, the substrate thickness is finite in practice. With the further increase in frequency, the mode would undergo a dispersive effect similar to that reported in the case of the standard CPW on ceramic substrate [14].

In the case of photoexcited CPW on semiconductor substrate, however, the validity of the quasi-TEM concept is attached to the further condition that the effective plasma depth d_e must be much smaller than the skin depth d_s, where $d_s \simeq [2/\omega\mu_0(\sigma_d + \Delta\sigma_e)]^{1/2}$. Otherwise, i.e., when the product of the frequency and the effective photoconductivity is large enough to yield $d_e \gtrsim d_s$, the excited CPW would behave in a way that is highly dispersive due to the skin effect.

A quantitative estimate of optically induced losses has been made for the case of small losses according to $G' \ll \omega C_r'$, which normally corresponds to the low-excitation condition $(\sigma_d + \Delta\sigma_e s/K) \ll \omega\epsilon_0\epsilon_r'$. This condition is usually satisfied over a wide range of irradiance (e.g. up to

[2]The agreement between theoretical and experimental results may be considered fairly satisfying with special regard to the fact that although the values of ϵ_r', σ_d, τ, L_a, and v_s used in this paper are from the substrate manufacturer and α_r and S were taken from literature, these values can differ considerably (partly up to 200 percent) from the actual parameter values of the test substrate. Moreover, the irradiances could be measured only with a 10 percent accuracy, and of course the actual substrate thickness was not infinite.

about 100 mW/cm^2 for high-resistivity silicon substrates) if the frequency is not too low. On the other hand, when applying stronger irradiances to operate the CPW under the high-excitation condition according to $\Delta\sigma_e s/K \gg \omega\epsilon_0\epsilon_r'$, the calculation of photoinduced attenuation can also be accomplished, in principle, by utilizing the TEM approach presented here. For this purpose, however, it is necessary to replace the "low-loss equation" (10) by a more general expression [10], [11], which finally implies a somewhat more complicated separation of α_d and α_{ph}. Moreover, normal operation of highly CW excited CPW's can only be achieved in conjunction with highly effective heat sinking.

In conclusion, the quasi-TEM approach allows a quantitative estimate of optically induced losses in CPW's on semiconductor substrate, varying the specific parameters of the substrate, the waveguide structure, and the light source. Preliminary experiments with a 50 Ω CPW transmission line section on 4000 Ω·cm silicon substrate were performed over the frequency range 1–18 GHz, applying 30 mW/cm^2 CW irradiance from a He–Ne laser as well as from an IR LED. The measured values of photoinduced attenuation constant agree fairly well with the theory, although the analysis reported here must be considered only approximate concerning the simplified incorporation of carrier diffusion and surface recombination effects and the disregard of finite-extent ground plane effects and test fixture influences.

Nevertheless, both the theoretical and experimental results give rise to the expectation that optically CW-induced attenuation up to 10 dB/cm or even more (without the need for excessive heat sinking) should be feasible, especially in regard to the continuous advance in the technology of high-CW-power laser diodes and LED's. Apart from the way of employing higher irradiances, a significant increase in attenuation can successfully be obtained by using substrates of higher carrier lifetime (e.g. silicon with $\tau = 10^{-4}$ s) in conjunction with smaller (optimized, $\delta \simeq 1$) CPW dimensions. From this aspect, the paper is understood as a useful contribution for the purpose of prompting further efforts in the development of optoelectronically controlled MIC devices, which are still far away from being mature at the present.

ACKNOWLEDGMENT

The authors gratefully acknowledge the assistance of G. Rohmer, S. Feuchtinger, and A. Seitzer. Thanks are also due to the referees for many helpful suggestions and for their constructive criticism.

REFERENCES

[1] W. Platte, "Optoelectronic microwave switching," in *Proc. Military Microwaves Conf.* (London), 1984, pp. 276–286; also *Proc. Inst. Elec. Eng.*, pt. J, vol. 132, pp. 126–132, 1985.

[2] A. M. Johnson and D. H. Auston, "Microwave switching by picosecond photoconductivity," *IEEE J. Quantum Electron.*, vol. QE-11, pp. 283–287, 1975.

[3] W. Platte, "Spectral dependence of microwave power transmission in laser-controlled solid-state microstrip switches," *Proc. Inst. Elec. Eng.*, pt. I, vol. 2, pp. 97–103, 1978.

[4] W. Platte, "Optoelectronic generation of short microwave bursts via pulse subtraction," *Arch. Elek. Ubertragung.*, vol. 32, pp. 377–378, 1978.

[5] D. H. Auston and P. R. Smith, "Generation and detection of millimeter waves by picosecond photoconductivity," *Appl. Phys. Lett.*, vol. 43, pp. 631–633, 1983.

[6] D. H. Auston, A. M. Johnson, P. R. Smith, and J. C. Bean, "Picosecond optoelectronic detection, sampling and correlation measurements in amorphous semiconductors," *Appl. Phys. Lett.*, vol. 37, pp. 371–373, 1980.

[7] P. Schmid and H. Melchior, "High-speed optoelectronic sampling with semiconductor-laser pulsed coplanar photoconductor," *Electron. Lett.*, vol. 20, pp. 684–685, 1984.

[8] D. E. Cooper and S. C. Moss, "Picosecond optoelectronic measurement of the high-frequency scattering parameters of a GaAs FET," *IEEE J. Quantum Electron.*, vol. QE-22, pp. 94–100, 1986.

[9] W. Platte, "Switched optoelectronic microwave load," *Proc. Inst. Elec. Eng.*, pt. I, vol. 129, pp. 193–198, 1982.

[10] W. Platte, *Mikrowellen-Optoelektronik, eine neue Technik zur Erzeugung kurzer Mikrowellenimpulse*. Düsseldorf: VDI-Verlag, 1986.

[11] W. Platte, "Optoelectronic microwave switching via laser-induced plasma tapers in GaAs microstrip sections," *IEEE Trans. Microwave Theory Tech.*, vol. MTT-29, pp. 1010–1018, 1981.

[12] C. P. Wen, "Coplanar waveguide: A surface strip transmission line suitable for nonreciprocal gyromagnetic device applications," *IEEE Trans. Microwave Theory Tech.*, vol. MTT-17, pp. 1087–1090, 1969.

[13] E. Jahnke, F. Emde, and F. Lösch, *Tables of Higher Functions*, 7th ed. Stuttgart: Teubner-Verlag, 1966.

[14] K. C. Gupta, R. Garg, and I. J. Bahl, *Microstrip Lines and Slotlines*. Dedham, MA: Artech House, 1979.

[15] W. Hilberg, "From approximations to exact relations for characteristic impedances," *IEEE Trans. Microwave Theory Tech.*, vol. MTT-17, pp. 259–265, 1969.

[16] M. Abramowitz and I. A. Stegun, Eds., *Handbook of Mathematical Functions*, 9th ed. New York: Dover, 1970.

[17] B. Sauerer and W. Platte, Internal Rep. IHFT-DA 440, Univ. of Erlangen–Nuernberg, Erlangen, West Germany, 1987.

[18] G. Rohmer and W. Platte, Internal Rep. IHFT-ST 441, Univ. of Erlangen–Nuernberg, Erlangen, West Germany, 1987.

[19] W. Platte, "Effective photoconductivity and plasma depth in optically quasi-CW controlled microwave switching devices," *Proc. Inst. Elec. Eng.*, pt. J, vol. 135, pp. 251–254, 1988.

[20] R. B. Adler, A. C. Smith, and R. L. Longini, "Introduction to semiconductor physics," in *Semiconductor Electronics Education Committee Books*, vol. 1. New York: Wiley, 1964.

[21] A. Ambroziak, *Semiconductor Photoelectric Devices*. London: Iliffe, 1968.

[22] W. Platte, "An optimization of semiconductor film thickness in light-controlled microstrip devices," *Solid-State Electron.*, vol. 20, pp. 57–60, 1977.

[23] P. F. Byrd and M. D. Friedman, *Handbook of Elliptic Integrals for Engineers and Physicists*. Berlin: Springer-Verlag, 1954.

[24] W. C. Dash and R. Newman, "Intrinsic optical absorption in single-crystal germanium and silicon at 77 K and 300 K," *Phys. Rev.*, vol. 99, pp. 1151–1155, 1955.

[25] W. Platte, "Photoinduced microwave attenuation in LED-controlled semiconductor coplanar waveguides," *Arch. Elek. Übertragung.*, to be published.

Walter Platte was born in Remscheid-Lennep, West Germany, on January 24, 1943. He received the Dipl.-Ing. degree in electrical engineering from the Technical University of Aachen, Aachen, West Germany, in 1968, the Dr.-Ing. degree in electrical engineering and the Habilitation degree ('venia legendi') from the University of Erlangen–Nuernberg, Erlangen, West Germany, in 1975 and 1986, respectively.

From 1968 to 1969, he worked at AEG-Telefunken, Ulm, West Germany, on *Ku*-band radar instrumentation and measurement, in particular Doppler radar moving target simulators. Since October 1969, he has been with the Department

of High-Frequency Techniques, University of Erlangen–Nuernberg, where he is engaged in research on laser-controlled MIC and mm-wave components, optoelectronics, optical communications, and fiber sensors. In addition, he has been lecturing on optical communication devices at the University of Erlangen–Nuernberg since 1977. In 1986, he was made an Adjunct Staff Member (Privat-Dozent) in the Faculty of Engineering Sciences at the university.

Dr. Platte is a member of the Verband Deutscher Elektrotechniker (VDE/NTG). He was awarded the Annual Prize of the Nachrichtentechnische Gesellschaft (NTG) in 1977, and the Finkelnburg-Habilitation-Prize of the University of Erlangen–Nuernberg in 1987.

Bernhard Sauerer was born in Regensburg, West Germany, on November 30, 1961. He received the Dipl.-Ing. degree in electrical engineering from the University of Erlangen–Nuernberg, Erlangen, West Germany, in 1987.

Since October 1987, he has been working in the Space Communications and Propulsion Systems Division at Messerschmitt-Boelkow-Blohm, Muenchen-Ottobrunn, West Germany, in the field of antenna research and development.